Hindawi
Shock and Vibration
Volume 2021, Article ID 5528555, 9 pages
https://doi.org/10.1155/2021/5528555

Research Article

Energy Variation Law and Rockburst Characteristics of Coal under Cyclic Loading

Hongjun Guo,[1,2] **Ming Ji**,[3] **Dapeng Liu**,[1] **Mengxi Liu**,[1] **Gaofeng Li**,[1] **Jingjing Chen**,[1] **and Hongjie Chen**[1]

[1]*Jiangsu Vocational Institute of Architectural Technology, Xuzhou 221116, China*
[2]*State Key Laboratory for Geomechanics & Deep Underground Engineering, China University of Mining & Technology, Xuzhou 221116, China*
[3]*Key Laboratory of Deep Coal Resource Mining, Ministry of Education of China, School of Mines, China University of Mining & Technology, Xuzhou 221116, China*

Correspondence should be addressed to Ming Ji; jiming@cumt.edu.cn

Received 14 April 2021; Accepted 17 May 2021; Published 25 May 2021

Academic Editor: Xiaowei Feng

Coal mining involves numerous challenges and safety risks owing to the complex engineering properties of coal bodies, which include discontinuities, heterogeneity, and anisotropy. In this paper, the strain energy during the coal deformation process is redivided in combination with cyclic loading and unloading tests to determine the energy evolution law and discuss the rockburst tendency characteristics. The results show that the elastic strain energy, and particularly the base-material strain energy, consistently dominates during the energy adjustment process, which is an important indicator of rockburst tendency. The elastic energy index and rebound deformation index also show that moderate plastic deformation (e.g., crack expansion and local penetration) can reduce the rockburst tendency level and prevent rockburst accidents. On the basis of the obtained results, precracking and pressure relief measures of blasting are adopted on site in advance of the working face, and good safety and economic benefits are achieved. These findings, thus, provide an important engineering reference for mines under similar conditions.

1. Introduction

Coal bodies are a special engineering rock mass with generally higher degrees of discontinuities, heterogeneity, and anisotropy than other rock types [1]. Coal bodies typically face complex genesis and stress environment conditions, large mining disturbances, and harsh production settings. Extensive research from a variety of perspectives has, therefore, aimed to comprehensively grasp the relevant characteristics of coal and effectively guide engineering practice, including studies on coal-rock interactions [2, 3], size effects [4, 5], bedding effects [6], gas content [7, 8], temperature [5, 9], water content [5, 10], fine and microcharacteristics [11–13], and acoustic emission characteristics [14, 15].

Remarkable progress has been achieved in recent years regarding the mechanical properties and energy evolution of coal under cyclic loading [16–22]. Yang et al. [2] established and discussed the energy-driving mechanism of combined coal-rock failure based on the mechanical response, energy evolution, and deformation and failure characteristics. Li et al. [23] studied the seepage and damage evolution characteristics of gas-bearing coal under three cyclic loading and unloading stress paths. Zhang et al. [15] characterized the damage evolution process of raw coal samples using acoustic emission positioning technology, proposed a time-space dimension cluster analysis method based on the *k*-means algorithm, and determined useful information regarding instability signs. Liu et al. [24] proposed that the elastic energy index of coal reaches a maximum at the elastic-plastic critical point when a rockburst is most likely to occur. Numerical calculation methods have also been used to study coal rockburst tendencies.

However, the abovementioned studies rarely addressed the influence of cracks on the energy evolution and rockburst characteristics of coal. Therefore, in this paper, the energy composition within coal bodies during the loading and unloading process is redivided considering the fracture strain energy [25], and the rockburst tendency characteristics are discussed on the basis of evolution law of each strain energy.

2. Experiment Overview

The coal sample used in the experiment was collected from the #8 coal seam in the third mining area of a mine in the Xianyang mining area and processed into standard cylinder specimens of Φ50 × H100 mm in accordance with national standards, as shown in Figure 1.

The experimental instrument is shown in Figure 2, and the specific method is as follows:

(1) Conventional uniaxial compression experiments: the average uniaxial compressive strength σ_c of the coal specimens is obtained by adopting the displacement control mode with a loading rate of 0.02 mm/s.

(2) Cyclic loading and unloading experiments: the displacement control mode and a loading/unloading rate of 0.02 mm/s are adopted. The change of σ_1 follows $0 \longrightarrow \sigma_0 \longrightarrow \sigma_u \longrightarrow \sigma_0 + d\sigma \longrightarrow \sigma_u \longrightarrow \sigma_0 + 2d\sigma \longrightarrow \ldots \longrightarrow \sigma_u \longrightarrow \sigma_0 + nd\sigma$, where $\sigma_0 = (75\%–80\%)\sigma_c$, $\sigma_u = (1\%–5\%)\sigma_c$, $d\sigma = 5\%\sigma_c$, and n is the cycles. This procedure is repeated until the coal sample is destroyed.

3. Classification and Calculation Method of Strain Energy

The specimen is only affected by the axial load of the test machine in the uniaxial cyclic loading and unloading experiments. Figure 3 shows the composition of the internal strain energy of the coal sample under one loading and unloading cycle, in which w_e and w_p are the elastic strain energy and plastic strain energy, respectively, and σ_{1+} and σ_{1-} are the loading stress and unloading stress.

The strain energy can be expressed as

$$\begin{cases} w = w_e + w_p, \\ w = \int_{\varepsilon_{p1}}^{\varepsilon_{e2}} \sigma_{1+} d\varepsilon_1, \\ w_e = \int_{\varepsilon_{e1}}^{\varepsilon_{e2}} \sigma_{1-} d\varepsilon_1, \end{cases} \tag{1}$$

where w is the total strain energy, and ε_p and ε_e satisfy

$$\begin{cases} \varepsilon_p = \varepsilon_{p2} - \varepsilon_{p1}, \\ \varepsilon_e = \varepsilon_{e2} - \varepsilon_{e1}, \end{cases} \quad \varepsilon_{p2} = \varepsilon_{e1}. \tag{2}$$

It can be seen from Figure 3 that the strain recovery rate is different during unloading, which is related to the random distribution of grains and fractures in the coal body. When the stress environment changes, the grains can respond quickly, while the fracture response lags behind, which is beneficial to understand the coal's dynamic failure [1]. Therefore, according to the composition and deformation characteristics of the coal body, the deformation can be divided into immediate recovery base-material deformation and delayed recovery fracture deformation (the internal cracks do not immediately change from compression to expansion). Figure 4 shows that the rebound deformation in the initial unloading stage is mainly base-material elastic deformation, which changes approximately linearly [25]. The section with good linear rebound is selected, and a tangent AC is drawn. The area of ABC is then the base-material strain energy w_g during the load cycle, that is,

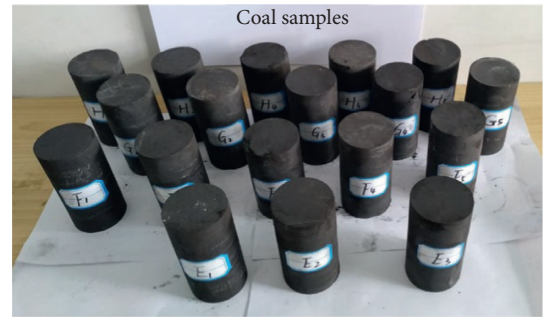

Figure 1: Coal samples.

Figure 2: SANS testing system at the China University of Mining and Technology.

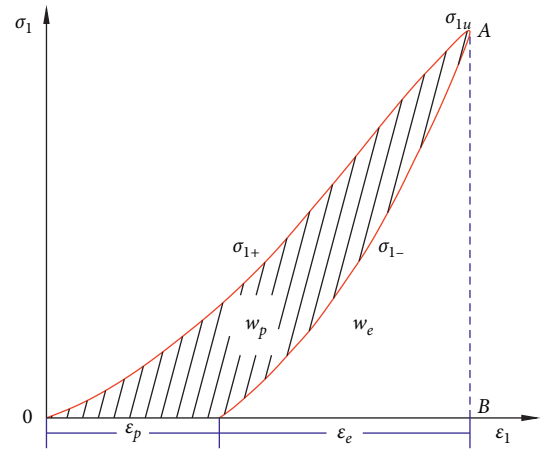

Figure 3: Internal strain energy of the coal sample.

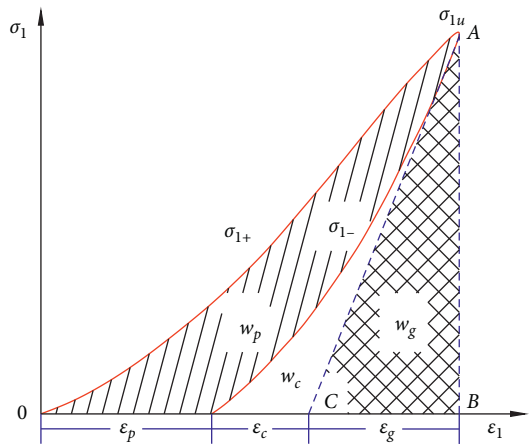

Figure 4: Classification and calculation of strain energy.

$$w_g = \frac{1}{2}\sigma_{1u}\varepsilon_g, \tag{3}$$

where σ_{1u} is the stress at an unloading point and ε_g is the reversible strain of the coal base-material.

The fracture strain energy w_c is then

$$w_c = w_e - w_g. \tag{4}$$

The relationship between the strain energy, stability, and rockburst tendency of coal under cyclic loading and unloading can be analyzed by equations (1)–(4).

4. Experiment Analysis and Discussion

4.1. Result Analysis. The stress-strain curves of the conventional uniaxial compression experiments are shown in Figure 5, yielding an average uniaxial compressive strength of 19.53 MPa.

According to the experimental scheme, 75% σ_c is selected as the initial unloading point. The stress-strain curves of each coal sample under cyclic loading and unloading are shown in Figure 6.

Figure 6 shows that specimens #1–#5 were destroyed after 12, 12, 4, 1, and 9 loading and unloading cycles, respectively. Specimens #1, #2, and #5 experienced more loading and unloading cycles and were, therefore, selected for further analysis to study the energy evolution in each cycle.

The strain energy is calculated using equations (1)–(4) according to the abovementioned classification and calculation method of strain energy. The energy-stress level curves are shown in Figure 7. The stress level represents the ratio of the load at each unloading point to the failure strength of the respective coal sample.

Figure 7 shows a consistent variation trend of the internal strain energy of each coal sample. The elastic strain energy increases with increasing stress level (i.e., number of cycles). Stress levels less than 90% increase approximately linearly, whereas the plastic strain energy initially decreases and then rapidly increases during the 1-2 loading and unloading cycles prior to failure. Additional changes are

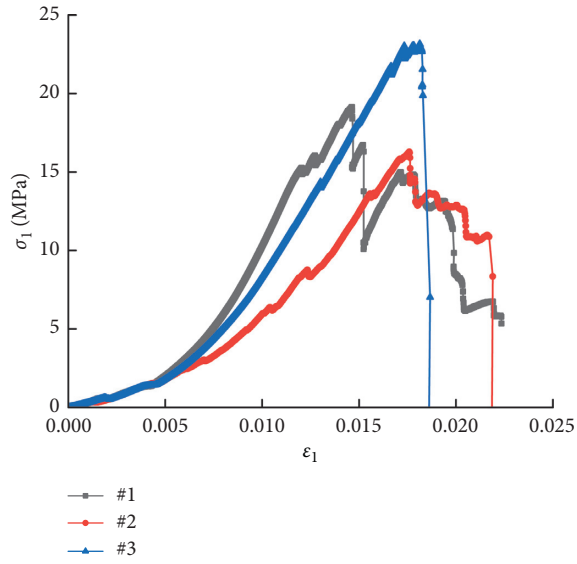

Figure 5: Stress-strain curves of the uniaxial compression experiments.

not substantial during the intermediate process, and base-material strain energy changes are close to those of the elastic strain energy. The change of fracture strain energy is not significant under low-stress conditions, but increases when the stress level exceeds 90%. It can, therefore, be concluded that the rapid change of each strain energy under high-stress conditions can be used as an indicator prior to coal failure.

The energy-ratio-stress-level curves are shown in Figure 8 to further explore the relationship between each strain energy and input energy.

Figure 8 shows that, in different loading and unloading cycles, approximately 80%–95% of the input energy is transformed into elastic strain energy. When the stress level exceeds 90% (i.e., 1-2 loading and unloading cycles prior to specimen failure), the elastic strain energy conversion rate significantly decreases, the plastic strain energy increases, and the coal enters the failure process, whereas within the elastic strain energy, the ratio of base-material strain energy to fracture strain energy essentially remains at 3–5:1. This indicates that the recovery of unloading deformation is mainly base-material rebound prior to failure.

4.2. Discussion and Application

4.2.1. Elastic Energy Index. Equation (5) is defined as the elastic energy index, which characterizes the rockburst tendency of coal and rock. Larger values are associated with higher rockburst tendencies. The values under different stress levels are shown in Figure 9.

$$W_{ET} = \frac{w_e}{w_p}. \tag{5}$$

Figure 9 shows that the elastic energy index roughly undergoes three processes with increasing stress level including a rapid increase and fluctuating increases and

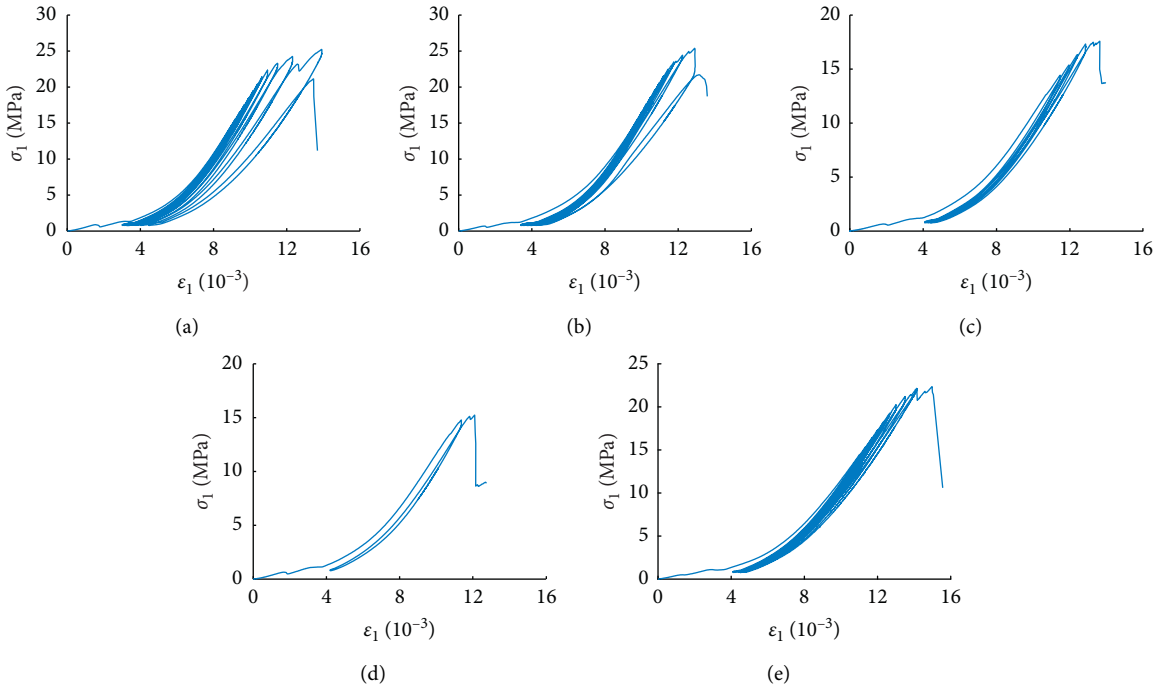

Figure 6: Stress-strain curves from cyclic loading and unloading. (a) #1. (b) #2. (c) #3. (d) #4. (e) #5.

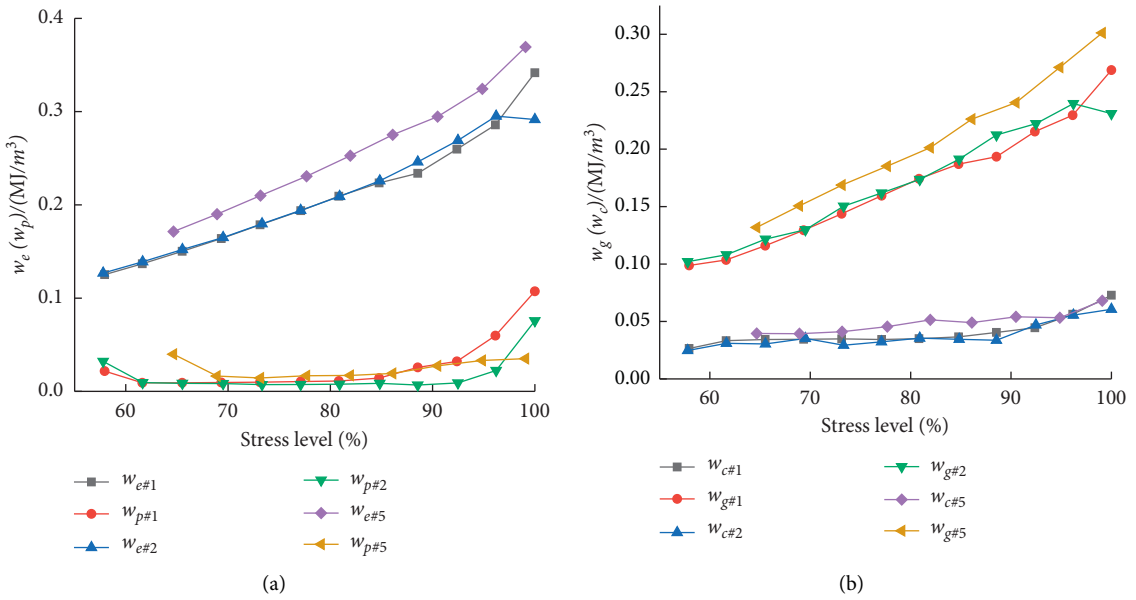

Figure 7: Energy-stress level curves.

decreases. This implies that the coal body has the highest rockburst tendency when it changes from the elastic to plastic state. Under continued loading and unloading, the energy consumption of the plastic deformation strongly increases, which reduces the brittleness and elastic energy index of the coal body, namely, the rockburst tendency decreases.

4.2.2. Rebound Deformation Index. Equation (6) is defined as rebound deformation index, which reflects the development degree of recoverable fractures in coal and rock and deformation recovery speed during the unloading process. Larger index values are associated with a lower degree of fracture development, faster rebound deformation, and higher rockburst tendency. The relationship with stress level is shown in Figure 10.

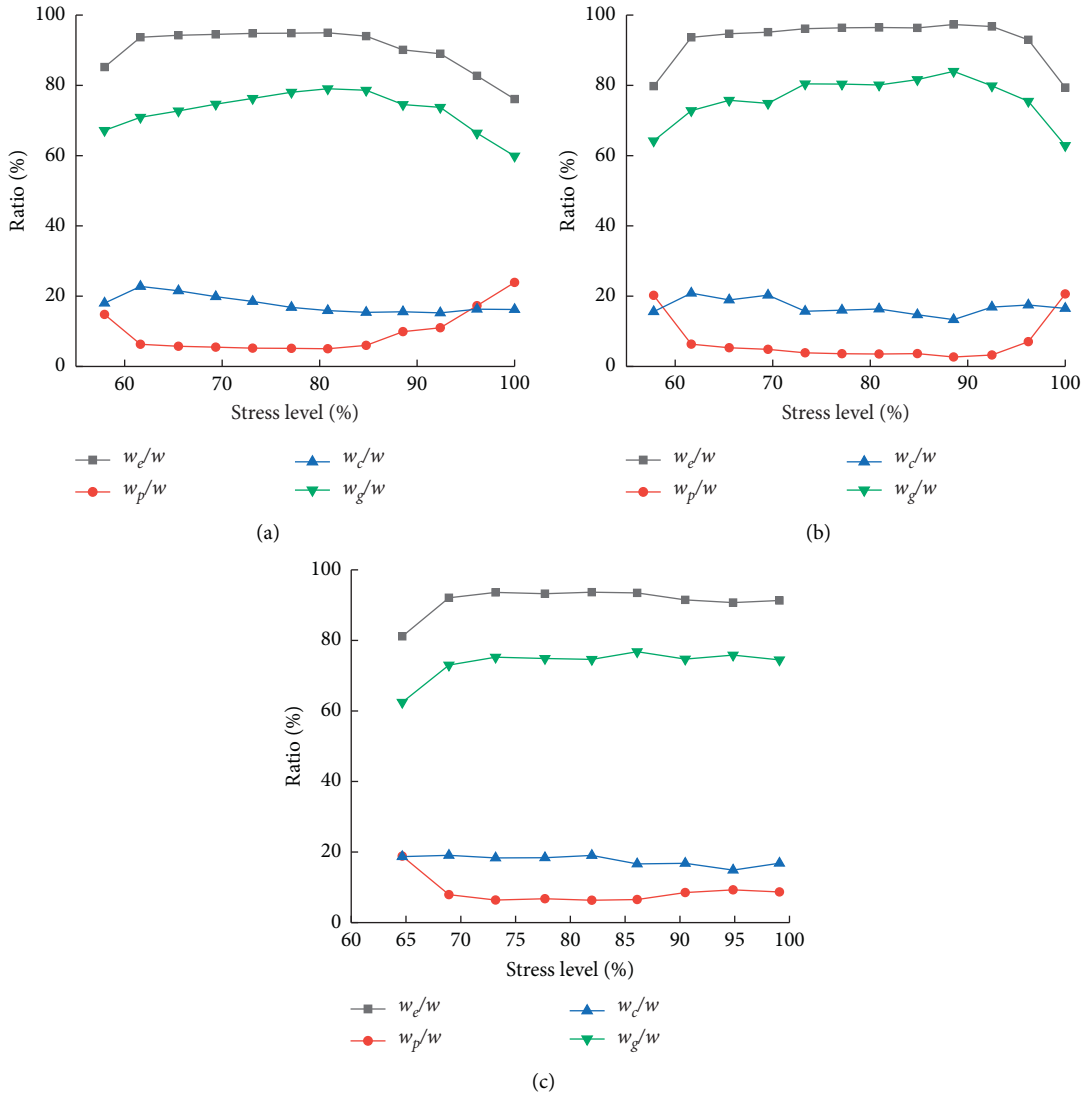

Figure 8: Relationship between the strain energy ratio and stress level. (a) #1. (b) #2. (c) #5.

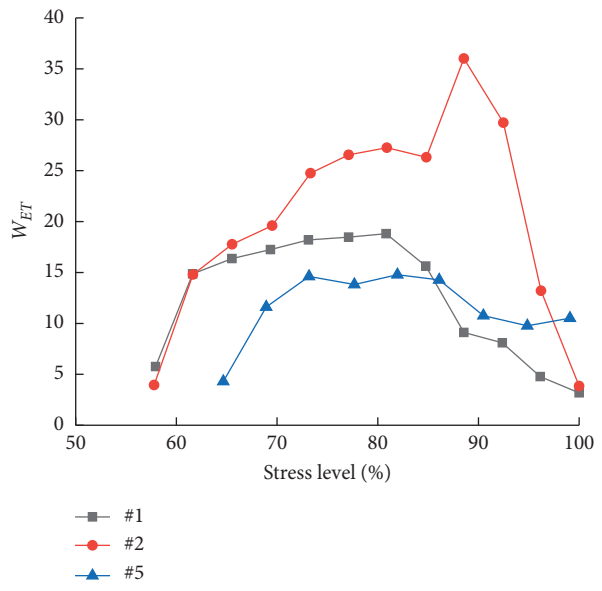

Figure 9: Relationship between the elastic energy index and stress level.

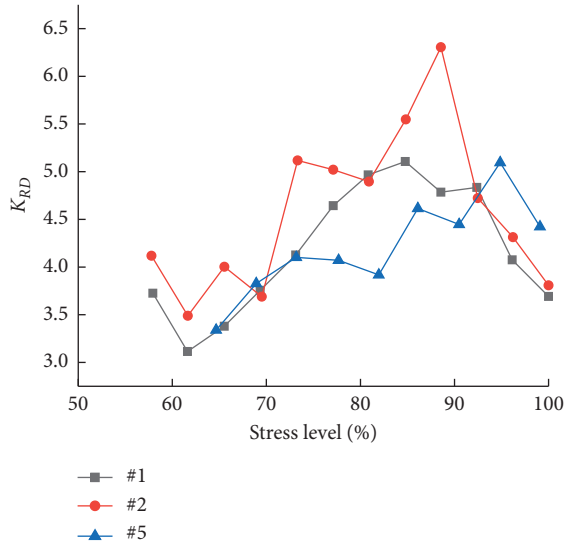

Figure 10: Relationship between the rebound deformation index and stress level.

Table 1: Measurement results of the coal seam rockburst tendency.

	D_T (ms)	W_{ET}	K_E	σ_c (MPa)
Measured results	1166.4	3.2	12.9	19.5
Evaluation interval	>500	2–5	>5	>14
Index rockburst category	I	II	III	III
Evaluation rank	III, strong rockburst tendency			

I- nonrockburst tendency; II- weak rockburst tendency; III- strong rockburst tendency.

Table 2: Statistics of roadway rockburst in the third mining area.

Frequency	Location of occurrence	Site description
1	Transportation roadway head-on 50 m backward	The floor heave is about 1 m, accompanied by dense and loud coal guns
2	Ventilation roadway corresponding to transportation roadway head-on 50 m forward	The floor heave is about 1.2 m, the roof is a seriously sinking or hanging bag, and many bolts (cables) in the roof and sides are broken, accompanied by dense and loud coal guns
3	Track roadway corresponding to transportation roadway head-on 50 m backward	The floor heave is about 0.5 m, one roof falls, and the bolts (cables) in the roof and sides are broken individually

The statistics covered a period of 22 days.

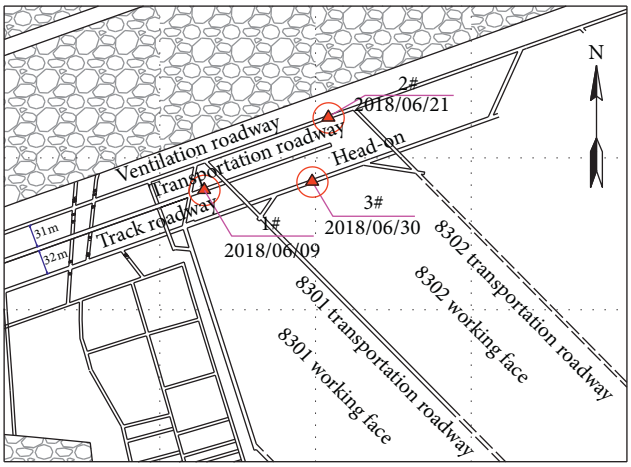

Figure 11: Diagram of the mining and excavation of the third mining area.

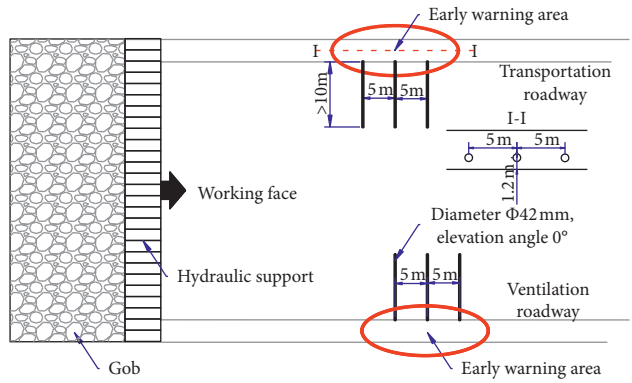

Figure 12: Blasting layout of the roadway side.

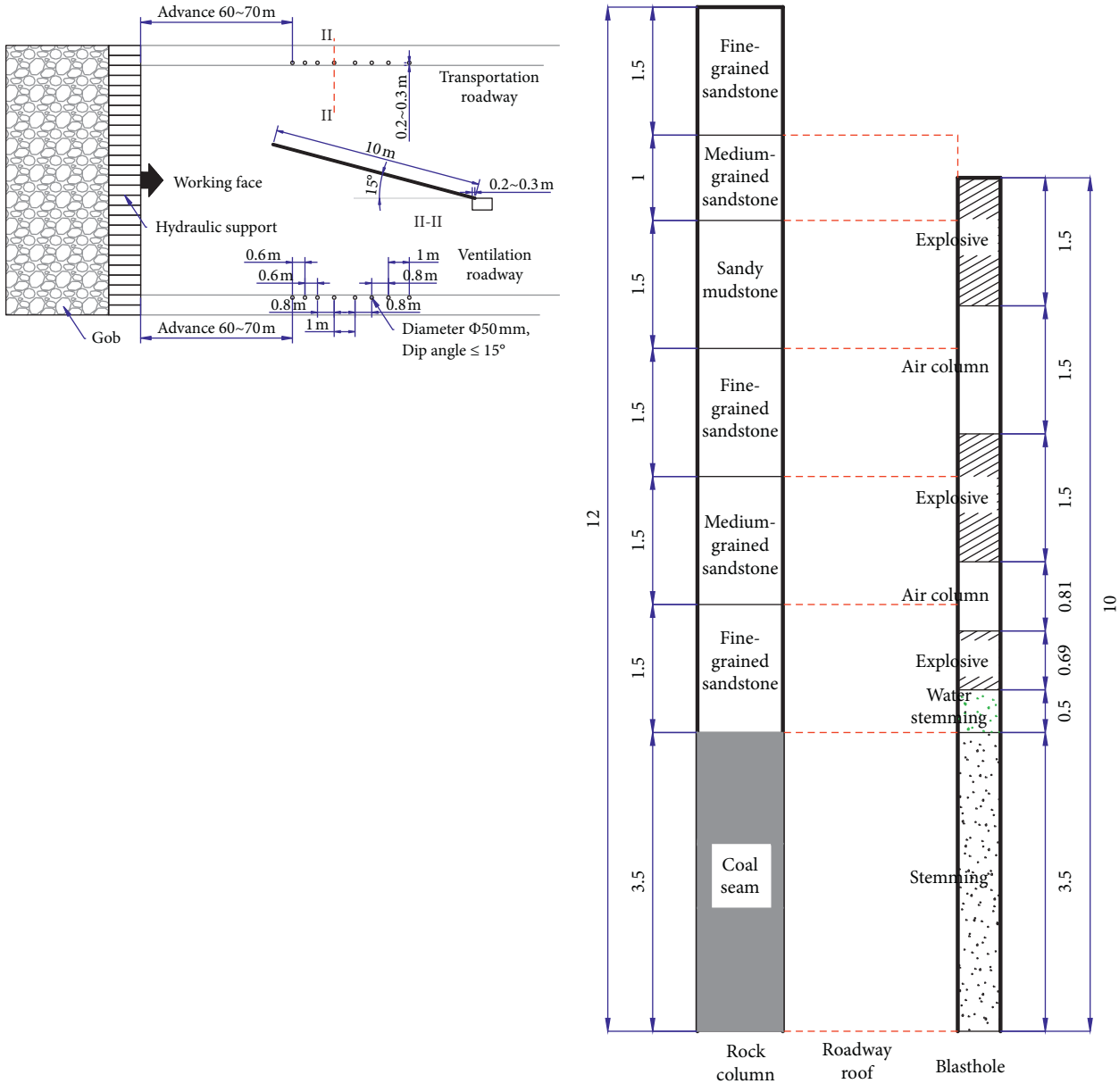

Figure 13: Blasting layout of the roadway roof. (a) Blasting layout of the roadway roof. (b) Charge design.

$$K_{RD} = \frac{w_g}{w_c}. \quad (6)$$

Figure 10 shows that the rebound deformation index remains essentially constant at 3–5 and that the unloading rebound is rapid. When the stress level exceeds 90%, the rebound deformation index value continuously decreases, which indicates that internal fractures have developed and expanded in the coal body, accompanied by partial crack coalescence and other irreversible deformation until the main crack forms. Before the coal body is destroyed, the low rebound deformation index state is beneficial for preventing and controlling rockburst accidents.

Table 1 lists the rockburst tendency indicators of the #8 coal seam.

The values in Table 1 indicate that the #8 coal seam has a high rockburst tendency and the elastic energy index is also notably lower than the value of each loading and unloading process in Figure 9. To some extent, this indicates that the coal seam has a high rockburst risk during mining and excavation disturbances in the production process, which is also confirmed by the statistics presented in Table 2. The rockburst location is shown in Figure 11.

The results indicate that, to reduce the influence of mining and excavation disturbances on the roadway and reduce or avoid rockburst accidents, part of the base-material strain energy that can be instantly released in the coal body is converted into fracture strain energy with a delayed release. This reduces the instantaneous release strength of the rockburst coal body and relieves the immediate danger. The blasting precracking and pressure relief measures in the advanced working face were measured at the study site, and the blasting layout of the coal body in the roadway mining side is shown in Figure 12. The roof blasting hole and charge design are shown in Figure 13 according to the structural characteristics of the roadway roof. The implementation effect is good, and safer mining and higher social and economic benefits are achieved.

5. Conclusions

Uniaxial cyclic loading and unloading experiments and a field study were performed to address the strain energy evolution of coal. The conclusions are summarized as follows:

(1) The composition of strain energy in a coal body during loading and unloading is redivided and calculated at different stress levels.

(2) The internal strain energy of each coal sample shows a consistent trend with increasing stress level (i.e., loading and unloading cycle). The elastic strain energy accounts for 80%–95% of the input energy, in which the base-material strain energy has a dominant advantage and both increase continuously. The plastic strain energy initially decreases, then fluctuates, and rises rapidly with increasing stress level. The fracture strain energy increases when the stress level exceeds 90%. The rapid change of each strain energy under high stress can be used as an indicator of coal failure.

(3) The elastic energy index and rebound deformation index reflect the rockburst tendency characteristics of coal to a certain extent, and moderate plastic deformation (e.g., crack expansion and local coalescence) is beneficial to prevent rockbursts.

(4) The safety and economic benefits of the field practice are good, which verifies the promising nature of the results obtained here and provides engineering guidance with substantial application value.

Data Availability

The data used to support the findings of the study are available from the corresponding author upon request.

Conflicts of Interest

The authors declare that there are no conflicts of interest regarding the publication of this paper.

Acknowledgments

This study was supported by Jiangsu University Natural Science Research Project (20KJB560032), Jiangsu University Natural Science Research Project (Key) (18KJA560001), Xuzhou Science and Technology Project (KC17156), and Jiangsu Construction System Science and Technology Project (Guidance) (2020ZD30, 2019ZD080, 2019ZD070, 2018ZD135, 2018ZD146, and 2018ZD170). The authors thank Esther Posner, PhD, from Liwen Bianji, Edanz Editing China (http://www.liwenbianji.cn/ac), for editing the English text of a draft of this manuscript.

References

[1] S. J. Wang, "Geological nature of rock and its deduction for rock mechanics," *Chinese Journal of Rock Mechanics and Engineering*, vol. 28, no. 3, pp. 433–450, 2009.

[2] L. Yang, F. Q. Gao, X. Q. Wang, and J. Z. Li, "Energy evolution law and failure mechanism of coal-rock combined specimen," *Journal of China Coal Society*, vol. 44, no. 12, pp. 3894–3902, 2019.

[3] Z. L. Mu, H. Wang, P. Peng, Z. J. Liu, and X. C. Yang, "Experimental research on failure characteristics and bursting liability of rock-coal-rock sample," *Journal of Mining and Safety Engineering*, vol. 30, no. 6, pp. 841–847, 2013.

[4] Y. K. Shi, Y. H. Ma, and Y. C. Yin, "Research on size effect affected to seam bump-prone test results," *Coal Science and Technology*, vol. 42, no. 2, pp. 23–26, 2014.

[5] H. J. Su, Q. Yin, H. W. Jing, and H. H. Zhao, "Research on bearing capacity and burst proneness of coal samples from western shallow-buried coal seam," *Journal of Mining and Safety Engineering*, vol. 32, no. 2, pp. 227–232+239, 2015.

[6] K. Y. Tian and C. Y. Luo, "Experimental and engineering practice on gas permeability characteristics in parallel and vertical bedding fractured coal body," *Journal of Natural Disasters*, vol. 29, no. 6, pp. 172–179, 2020.

[7] G. H. Zhang, Z. H. OoYang, Q. X. Qi, H. Y. Li, Z. G. Deng, and J. J. Jiang, "Experimental research on the influence of gas on

coal burst tendency," *Journal of China Coal Society*, vol. 42, no. 12, pp. 3159–3165, 2017.

[8] H. G. Xu and W. J. Liu, "Study on temperature change characteristics of coal gas adsorption-desorption process based on infrared measurement," *Coal Mine Modernization*, vol. 1, pp. 124–128, 2021.

[9] X. Cui, L. W. Guo, J. Y. Zhang, and J. Jia, "Study on the influence range of heat release of coal seam expansion permeability enhanced material on coal mass," *Mining Safety & Environmental Protection*, vol. 48, no. 1, pp. 6–10, 2021.

[10] P. Y. Su and J. Jia, "Study on the influence of surrounding rock pressure and water content on the permeability of coal body," *Shanxi Science Technology*, vol. 35, no. 6, pp. 31–34, 2020.

[11] B. Li, L. S. Huang, Y. J. Ren, and M. S. Jiang, "Experimental study on meso-structure change and phase-transforming fracturing of coal under low temperature," *Journal of Safety Science and Technology*, vol. 16, no. 7, pp. 25–29, 2020.

[12] D. K. Wang, P. Zhang, J. P. Wei, Y. Wu, and F. C. Zeng, "Research on dynamic evolution of 3D Fracture Structure Of Loaded Coal Body Based on CT visualization," *Journal of China Coal Society*, vol. 44, no. S2, pp. 574–584, 2019.

[13] B. Li, J. B. Liu, J. G. Ren, F. Chen, and Z. M. Song, "Experimental study of the influence of hydraulic punching on the microscopic pore and structural components of coal," *Coal science and Technology*, pp. 1–9, 2021.

[14] H. Y. Li, Z. X. Sun, Q. X. Qi, F. M. Li, and S. K. Zhao, "Deformation rules and acoustic emission characteristics of coal with different outburst proneness," *Journal of Liaoning Technical University (Natural Science)*, vol. 36, no. 12, pp. 1251–1256, 2017.

[15] Z. B. Zhang, S. J. Li, E. Y. Wang, X. A. Liu, and Y. H. Zhang, "Research on the damage evolution characteristics of coal based on cluster analysis of temporal-spatial dimension of acoustic emission events," *Chinese Journal of Rock Mechanics and Engineering*, vol. 39, no. S2, pp. 3338–3347, 2020.

[16] H. Wang and J. Li, "Mechanical behavior evolution and damage characterization of coal under different cyclic engineering loading," *Geofluids*, vol. 2020, Article ID 8812188, 19 pages, 2020.

[17] H. Duan and D. Ma, "Acoustic emission simulation on coal specimen subjected to cyclic loading," *Advances in Civil Engineering*, vol. 2020, Article ID 3798292, 17 pages, 2020.

[18] K. Peng, S. Shi, Q. Zou et al., "Characteristics of energy storage and dissipation of coal under one-time cyclic load," *Energy Science & Engineering*, vol. 8, no. 9, pp. 3117–3135, 2020.

[19] Q. Li, Y. Liang, Q. Zou, and Q. Li, "Acoustic emission and energy dissipation characteristics of gas-bearing coal samples under different cyclic loading paths," *Natural Resources Research*, vol. 29, no. 2, pp. 1397–1412, 2020.

[20] Z. Z. Zhang, M. Deng, J. B. Bai, X. Y. Yu, Q. H. Wu, and L. S. Jiang, "Strain energy evolution and conversion under triaxial unloading confining pressure tests due to gob-side entry retained," *International Journal of Rock Mechanics and Mining Sciences*, vol. 126, Article ID 104184, 2020.

[21] L. Fan and S. M. Liu, "Evaluation of permeability damage for stressed coal with cyclic loading: an experimental study," *International Journal of Coal Geology*, vol. 216, pp. 1–13, Article ID 103338, 2019.

[22] H. Guo, M. Ji, Y. Zhang, and M. Zhang, "Study of mechanical property of rock under uniaxial cyclic loading and unloading," *Advances in Civil Engineering*, vol. 2018, Article ID 1670180, 6 pages, 2018.

[23] Q. M. Li, Y. P. Liang, and Q. L. Zou, "Seepage and damage evolution characteristics of different gas-bearing coal under cyclic loading-unloading conditions," *Journal of China Coal Society*, vol. 44, no. 9, pp. 2803–2815, 2019.

[24] J. W. Liu, B. X. Huang, and M. T. Wei, "Influence of cyclic uniaxial loading on coal elastic-plastic properties and energy accumulation and dissipation," *Journal of Liaoning Technical University (Natural Science)*, vol. 31, no. 1, pp. 26–30, 2012.

[25] H. Fu, S. Wang, X. Pei, and W. Chen, "Indices to determine the reliability of rocks under fatigue load based on strain energy method," *Applied Sciences*, vol. 9, no. 3, p. 360, 2019.